Atherosclerosis 387 (2023) 117387

Contents lists available at ScienceDirect

Atherosclerosis

journal homepage: www.elsevier.com/locate/atherosclerosis

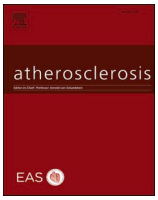

Mechanical wall stress and wall shear stress are associated with atherosclerosis development in non-calcified coronary segments

Aikaterini Tziotziou [a], Eline Hartman [a,b], Suze-Anne Korteland [a], Aad van der Lugt [c], Antonius F.W. van der Steen [a], Joost Daemen [b], Daniel Bos [c,d], Jolanda Wentzel [a], Ali C. Akyildiz [a,e,*]

[a] Department of Biomedical Engineering, Erasmus Medical Center, Rotterdam, the Netherlands
[b] Department of Cardiology, Erasmus Medical Center, Rotterdam, the Netherlands
[c] Department of Radiology & Nuclear Medicine, Erasmus Medical Center, Rotterdam, the Netherlands
[d] Department of Epidemiology, Erasmus Medical Center, Rotterdam, the Netherlands
[e] Department of Biomechanical Engineering, Delft University of Technology, Delft, the Netherlands

ARTICLE INFO

Keywords:
Coronary
Atherosclerosis
Mechanical stress
Shear stress
NIRS-IVUS and OCT

ABSTRACT

Background and aims: Atherosclerotic plaque onset and progression are known to be affected by local biomechanical factors. While the role of wall shear stress (WSS) has been studied, the impact of another biomechanical factor, namely mechanical wall stress (MWS), remains poorly understood. In this study, we investigated the association of MWS, independently and combined with WSS, towards atherosclerosis in coronary arteries.

Methods: Thirty-four human coronary arteries were analyzed using near-infrared spectroscopy intravascular ultrasound (NIRS-IVUS) and optical coherence tomography (OCT) at baseline and after 12 months. Baseline WSS and MWS were calculated using computational models, and wall thickness (ΔWT) and lipid-rich necrotic core size (ΔLRNC) change were measured in non-calcified coronary segments. The arteries were further divided into 1.5 mm/45° sectors and categorized as plaque-free or plaque sectors. For each category, associations between biomechanical factors (WSS & MWS) and changes in coronary wall (ΔWT & ΔLRNC) were studied using linear mixed models.

Results: In plaque-free sectors, higher MWS ($p < 0.001$) was associated with greater vessel wall growth. Plaque sectors demonstrated wall thickness reduction over time, likely due to medical therapy, where higher levels of WSS and WMS, individually and combined, ($p < 0.05$) were associated with a greater reduction. Sectors with low MWS combined with high WSS demonstrated the highest LRNC increase ($p < 0.01$).

Conclusions: In this study, we investigated the association of the (largely-overlooked) biomechanical factor MWS with coronary atherosclerosis, individually and combined with WSS. Our results demonstrated that both MWS and WSS significantly correlate with atherosclerotic plaque initiation and development.

1. Introduction

The focal distribution and compositional variation of atherosclerotic plaques along the coronary tree suggest local differences in susceptibility to atherosclerosis [1–3]. Biomechanical factors are among the local risk factors that play a crucial role in the onset, progression, and compositional change of atherosclerotic plaques [4].

Two important biomechanical factors effective in arterial circulation are blood flow-induced wall shear stress (WSS) and blood pressure-induced mechanical wall stress (MWS) [4]. WSS is the biomechanical stress due to the frictional force exerted by the blood flow on endothelial cells, parallel to the arterial lumen surface. Sensitivity of endothelial cells to changes in WSS levels can result in activation of inflammatory pathways [5], such as downregulation of nitric oxide, leading to plaque initiation [6]. Moreover, non-physiological WSS has been shown to correlate with plaque growth and destabilization [7–10].

The other biomechanical factor, MWS, is the structural stress inside the arterial wall due to blood pressure and is greatly affected by local arterial geometry [11,12]. MWS causes stretch and expansion of the arterial wall and endothelial cells [13]. In respect of atherosclerosis,

* Corresponding author. Department of Biomedical Engineering, Erasmus Medical Center, Rotterdam, the Netherlands.
E-mail address: a.akyildiz@erasmusmc.nl (A.C. Akyildiz).

https://doi.org/10.1016/j.atherosclerosis.2023.117387
Received 22 June 2023; Received in revised form 9 November 2023; Accepted 10 November 2023
Available online 15 November 2023

MWS has mainly been studied in relation to plaque rupture [14–18]. However, the association of MWS with plaque formation and development has received limited attention although high MWS is known to activate numerous inflammatory pathways and promote extracellular matrix synthesis in the arterial wall, by local Angiotensin II production, causing wall thickening under hypertensive conditions [19,20].

To have a more comprehensive understanding of the involvement of biomechanics in coronary atherosclerosis, we studied the individual and combined effects of MWS and WSS in plaque-free and plaque sectors of atherosclerotic coronaries. Artery-specific computational models of human coronary arteries were constructed to assess MWS and WSS, which are in the end used to examine their influence on coronary atherosclerosis.

2. Patients and methods

2.1. Study design

This study was embedded within the prospective single-center observation cohort study [21] performed at the Erasmus University Medical Center, Rotterdam, the Netherlands. According to the protocol inclusion criteria, the study included patients (n = 53) who presented with acute coronary syndrome, were hemodynamically stable, and had at least one non-stented, non-culprit coronary artery, subject to invasive imaging and physiology measurements. Patients with coronary artery bypass graft surgery, 3-vessel disease, renal insufficiency, left ventricular ejection fraction <30% and atrial fibrillation were not included in the study. All patients agreed to participate in the study and provided written informed consent. The study protocol was approved by the local medical ethics committee of Erasmus University Medical Center (MEC 2015- 535, NL54519.078.15), and the study was conducted in accordance with the World Medical Association Declaration of Helsinki (64th WMA General Assembly, Fortaleza, Brazil, October 2013) and Medical Research Involving Human Subject Act (WMO). Details of the image acquisition protocol, the patient inclusion/exclusion criteria, and the informed consent can be found in a previous publication of our group [21].

2.2. Data acquisition

Imaging of a non-culprit artery, either a left circumflex (LCX), a left anterior descending (LAD), or a right coronary artery (RCA), was performed following successful treatment of the culprit vessel (baseline time point). Complete optical coherence tomography (OCT) by an automated pullback (36 mm/s) (Dragonfly Optics Imaging Catheter, St Jude Medical, St Paul, MN, USA) and serial near-infrared spectroscopy intravascular ultrasound (NIRS-IVUS) by an automated pullback (0.5 mm/s) (TVC, InfraReDx, Burlington, Massachusetts, USA) were obtained in 53 non-stented, non-culprit coronary segments. One month after the index procedure, patients visited the outpatient clinic to undergo a coronary computed tomography angiogram (CCTA) according to a standard prospectively ECG-triggered clinical protocol (SOMATOM Force (3rd generation dual-source CT scanner), (Siemens Healthineers, Germany). The same arteries were imaged for the second time 12 months later (follow-up time point) (Fig. 1). All arterial segments

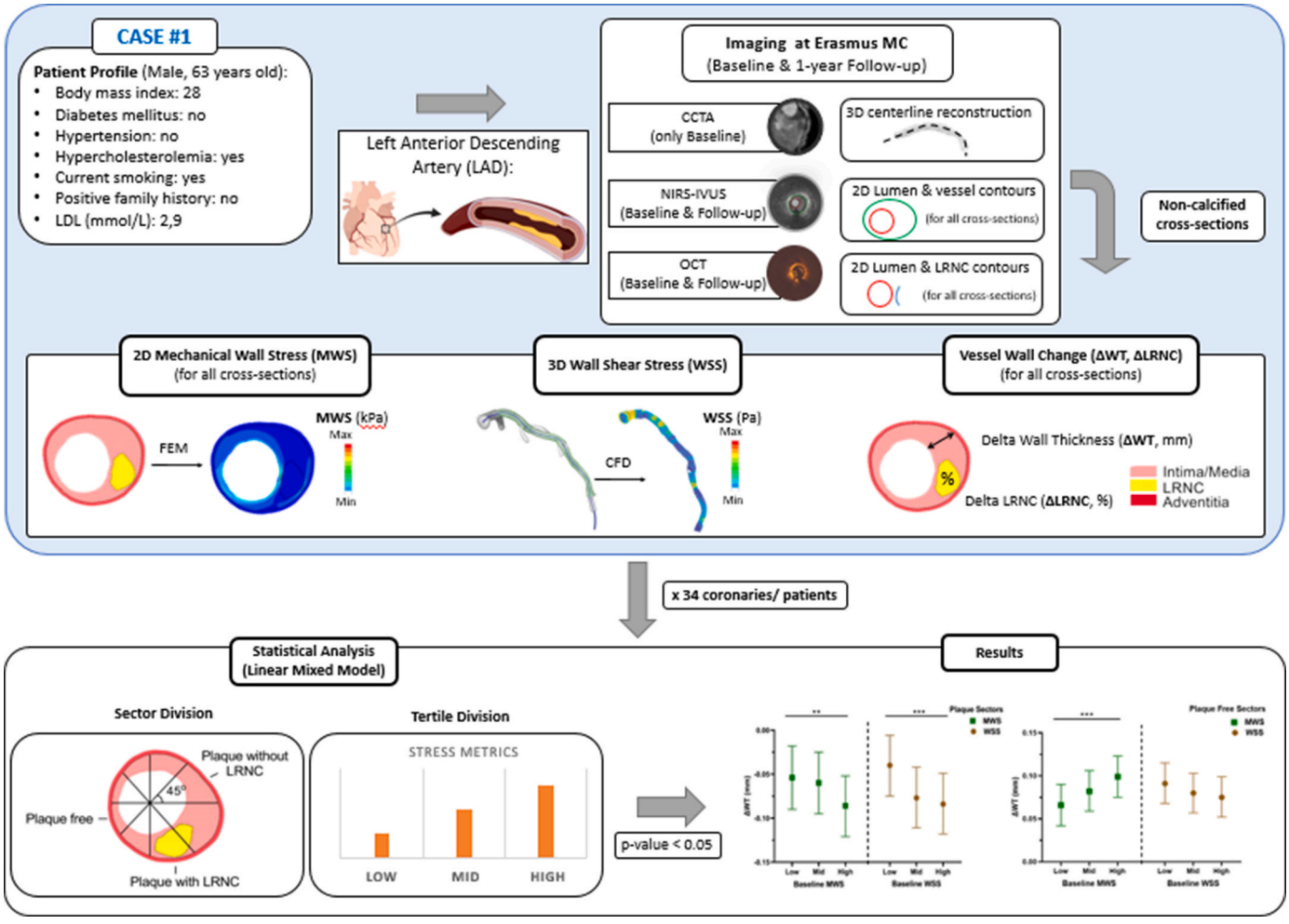

Fig. 1. Study design pipeline with case example.

selected for the study were at least 30 mm long. Blood flow and pressure were measured within each segment using a ComboWire (Philips Volcano, Rancho Cordova, CA, USA) [21].

2.3. Wall shear stress assessment at baseline

2.3.1. Lumen geometry construction

3D lumen geometries were constructed from IVUS and CCTA imaging baseline data. The gated IVUS frames were selected six frames before the R-peak of the echocardiogram in the end-diastolic phase to avoid lumen inaccuracies due to constant IVUS pullback and cardiac motion, using in-house developed MATLAB (v.2017B, Mathworks Inc, USA) code [21]. The lumen contours at baseline and follow-up were segmented on the NIRS-IVUS frames [21]. CCTA scans were only available at baseline and used for reconstruction of coronary centerlines. Positive NIRS signal indicated a high probability of lipid-rich necrotic core (LRNC) presence, and the NIRS-IVUS data with the CCTA-derived coronary centerline were reconstructed using coronary side branches as landmarks in MeVisLab (MeVis Medical Solutions AG, Bremen, Germany) [21,22].

2.3.2. Computational fluid dynamics analysis

Wall shear stress (WSS) was computed in these 3D lumen reconstructions of the coronary arteries with Computational Fluid Dynamics (CFD) and was reported previously [21]. Briefly, time-dependent CFD simulations (Fluent, v.17.1, ANSYS Inc.) were performed for all coronaries imaged, by implementing blood as an incompressible, homogeneous Carreau fluid, and walls were assumed to be rigid. Artery-specific inlet and outlet flow boundary conditions were prescribed based on patient-specific Doppler flow measurements. WSS for the entire 3D coronary geometry over a cardiac cycle was computed for all coronaries (Fig. 1). Time-averaged wall shear stress was reported in this manuscript and simply referred to as WSS in the rest of the manuscript.

2.4. Mechanical wall stress at baseline

2.4.1. Cross-sectional wall geometry and composition

2D coronary cross-sections were generated based on the combined and co-registered baseline NIRS-IVUS and OCT frames at every 1 mm. A complete co-registration of the NIRS-IVUS and OCT frames was achieved via an in-house developed MATLAB code. At least two coronary side branches visible in both imaging modalities were used as natural landmarks for longitudinal and circumferential co-registration. The outer vessel wall geometry was constructed from IVUS images. Since the outermost structure visible on IVUS frames was the external elastic lamina (EEL), a layer of 0.15 mm uniform thickness [12] was added around the EEL to account for the mechanical contribution of the adventitia layer in the computational models. Regions with calcification were excluded from the study as they impeded the segmentation of EEL [21]. The reconstruction of the LRNC was accomplished using an algorithm developed and validated previously by our group [23], as the outer edge of LRNC was not visible in IVUS or OCT.

2.4.2. Finite element modeling analysis

Finite Element (FE) modeling approach was used to compute the mechanical wall stress (MWS) [11,12]. First, the 2D cross-sectional geometries were transferred to the FE modeling software ABAQUS (2019, Dassault Systemes) (Fig. 1). Isotropic, nonlinear, hyperelastic, and incompressible material models were used for the intima/media, adventitia, and LRNC components [4,11,12]. Since the coronary geometries were obtained when the arteries were under a certain blood pressure and not at zero mechanical load, the backward incremental method [11] was used to compute the initial stresses, which were present at the time of artery imaging. Artery-specific blood pressure, measured with the ComboWire, was used in the computations. The FE analyses were performed under plane strain condition. Mesh sensitivity analysis was performed to ensure the independency of the stress results on the model mesh. On average, 5000 elements of CPE3H (3-node linear plane strain triangle, hybrid, constant pressure) type per cross-section were employed. MWS, more specifically von Mises stress, was outputted from the FE simulations. Maximum luminal MWS and the average MWS within the vessel wall are reported here in this manuscript.

2.5. Change in vessel wall thickness and composition

The vessel wall change was quantified by measuring the intima/media tissue thickness (distance between the lumen and the EEL) on both baseline and follow-up NIRS-IVUS frames. The thickness change was reported in the manuscript as wall thickness change (ΔWT). The compositional change was assessed with the LRNC percentage change, based on NIRS positive measurements, and reported as LRNC percentage change (ΔLRNC) (Fig. 1).

2.6. Statistical analysis

To study the local effects, the arterial segments were divided into sectors that span an angle of 45° in the circumferential direction and a length of 1.5 mm in the longitudinal direction (Fig. 1) in order to perform local stress analysis and locate the shape and size of LRNC. Cross-sections at the side-branch locations were excluded from further analyses due to the incomplete intactness in the circumference. The sectors then were categorized as either plaque-free sectors (mean WT $<$0.5 mm) or plaque sectors (mean WT $>$0.5 mm) with LRNC (NIRS + percentage $>$ 50%) or without LRNC (NIRS + percentage $<$ 50%), as illustrated in Fig. 1 [21]. WT and LRNC percentages were quantified per sector. The analyses were performed separately for plaque-free and plaque sectors.

For the statistical analysis, WSS and MWS values per sector type (plaque-free vs. plaque sectors) were divided into tertiles (low, mid, and high). For plaque-free sectors, the thresholds to define the tertiles were 0.53 Pa (low-mid) and 1.07 Pa (mid-high) for WSS, 157 kPa (low-mid) and 372 kPa (mid-high) for luminal MWS, and 62.5 kPa (low-mid) and 133.6 kPa (mid-high) for within wall MWS. For the plaque sectors, the threshold values were 0.7 Pa (low-mid) and 1.29 Pa (mid-high) for WSS, 58.3 kPa (low-mid) and 105.6 kPa (mid-high) for luminal MWS, and 22.2 kPa (low-mid) and 34.5 kPa (mid-high) for within wall MWS.

Linear regression analysis was used to evaluate the association between baseline WSS and MWS, both luminal and within the vessel wall, in both plaque-free and plaque sectors. The association of baseline WSS tertiles and baseline MWS tertiles, both luminal and within the vessel wall, with follow-up WT and LRNC percentages at the sector level was evaluated using Linear Mixed Models to account for the intra-artery correlations of the segments. The stress metrics, the NIRS presence, and their interaction were implemented as fixed factors, and the individual vessels as random factors while correcting for the baseline WT, statin treatment and cardiovascular risk factors including diabetes, hypertension, hypercholesterolemia, smoking, obesity and positive family history. The ΔWT and ΔLRNC were calculated by subtracting the corrected baseline WT and LRNC percentages from the estimated follow-up WT and LRNC percentages, respectively. SPSS (IBM SPSS 27 Software, Armonk, New York) was used for statistical analyses, and $p < 0.05$ was considered significant.

3. Results

3.1. Vessel characteristics at the baseline

From the 53 non-culprit coronaries, 19 had to be excluded from further analysis, because of either consent withdrawal or missing/low-quality imaging or pressure data (Fig. 2). The final analysis included 34 coronaries from 34 patients, whose baseline characteristics are

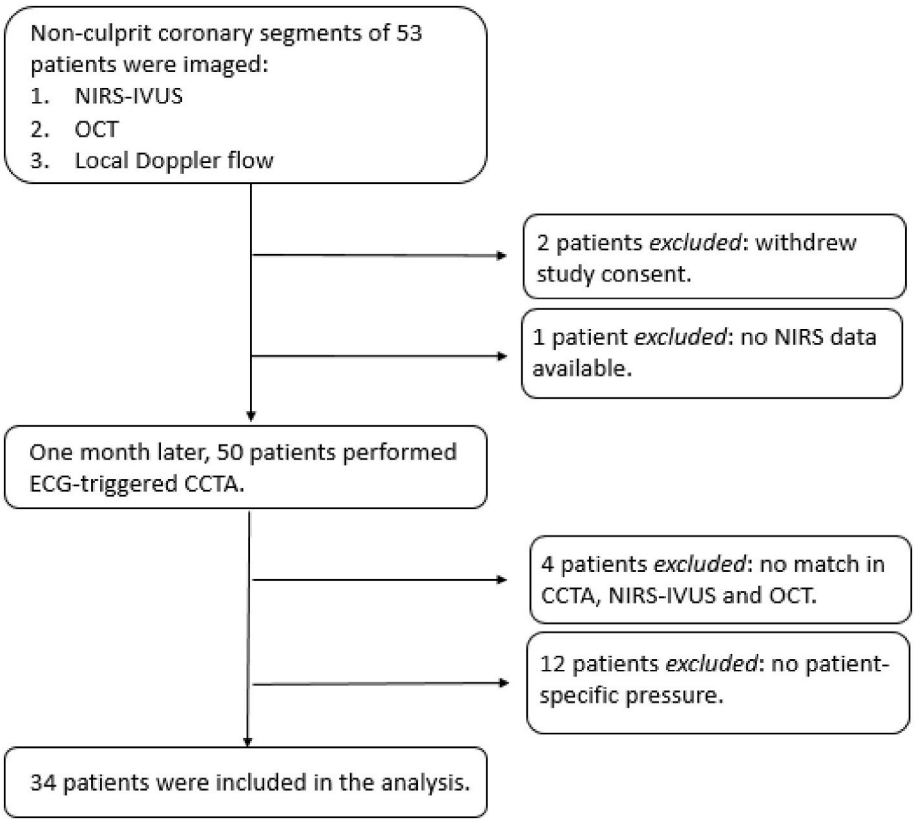

Fig. 2. Flowchart of the study design protocol with data acquisition information.

provided in Table 1. Seventeen patients were under statin treatment at the time of inclusion, another fifteen started statin therapy within a month and the other two at sixth and eleventh month after the first coronary imaging. All patients were under statin treatment at the follow-up time point.

From the 34 coronary arteries imaged (13 LADs, 11 RCAs, and 10 LCXs), 6527 sectors were analyzed. At baseline, 63% (n = 4112) of the analyzed sectors were identified as plaque-free. The rest were identified as plaque sectors (n = 2415), of which 22% contained LRNC tissue. The median (range) baseline WT of plaque-free sectors was 0.23 mm (0.02–0.49 mm) while the plaque sectors had a median WT of 0.70 mm (0.50–2.06 mm). Plaque sectors with and without LRNC presented baseline WT of 0.76 mm (0.50–2.06 mm) and 0.67 mm (0.50–1.91 mm), respectively.

3.2. Wall thickness change and biomechanics

3.2.1. Plaque-free sectors

Over the one-year study period, plaque-free sectors had a mean ΔWT of 0.06 mm, 95% CI [0.05, 0.07], where 63% of the sectors showed an increase in thickness over time. More detailed WT measurements at baseline and follow-up are provided in Supplementary data.

Regression analyses showed no correlation between WSS and luminal MWS ($R^2 = 0.015$) or within-vessel MWS ($R^2 = 0.020$), whereas luminal MWS and within-vessel MWS were correlated ($R^2 = 0.61$) and demonstrated similar stress distribution results. Therefore, only WSS and luminal MWS were used for further statistical analyses. Luminal MWS was preferred over within-vessel MWS in the analyses since the attention of plaque remodeling, progression and vulnerability studies so far has mainly focused on the luminal region. The statistical analyses based on linear mixed models (with WSS, luminal MWS, and the interactions thereof as fixed factors while correcting for baseline WT) revealed a significant positive association between baseline luminal MWS and ΔWT ($p < 0.001$) in the plaque-free sectors, where higher levels of baseline luminal MWS showed higher mean ΔWT over time (Fig. 3A). Contrarily, a negative trend was observed between baseline WSS and ΔWT, where the sectors exposed to lower WSS demonstrated higher ΔWT over time (Fig. 3A). This association between baseline WSS and ΔWT was almost statistically significant ($p = 0.058$).

Table 1
Patients' characteristics at baseline.

Baseline patients characteristics (n = 34)	
Age (years):	62 ± 8.9
Men, n (%):	31 (91.2%)
Body mass index:	27 ± 4.6
Diabetes mellitus, n (%):	6 (17.6%)
Hypertension, n (%):	8 (23.5%)
Hypercholesterolemia, n (%):	15 (44.1%)
Current smoking, n (%)	6 (17.6%)
Positive family history, n (%):	13 (38.2%)
Previous MI, n (%):	7 (21.6%)
Previous PCI, n (%):	8 (24.3%)
LDL (mmol/L):	2.6 (2.1–3.2)

3.2.2. Plaque sectors

Plaque sectors showed a mean ΔWT of −0.07 mm, 95% CI [-0.08, −0.06], where 67% of the sectors demonstrated a decrease in thickness over time. More detailed WT measurements at baseline and follow-up are provided in the Supplementary data.

WSS was not correlated to luminal MWS ($R^2 = 0.006$) or within-vessel MWS ($R^2 = 0.017$). Luminal MWS and within-vessel MWS were moderately correlated ($R^2 = 0.32$). Based on the statistical analyses with linear mixed models (with WSS, luminal MWS, within vessel MWS, LRNC presence and interactions thereof were fixed factors while correcting for baseline WT), only LRNC presence, WSS, luminal MWS and the interaction term of the three were statistically significant for ΔWT.

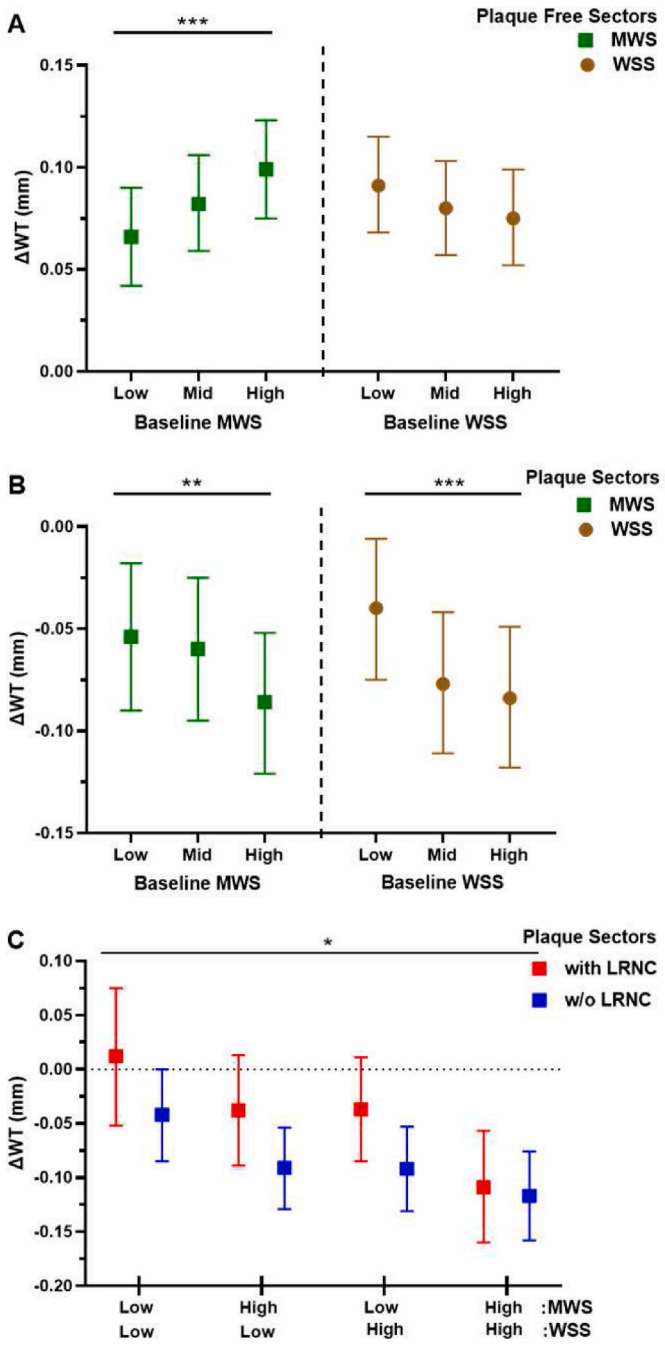

Fig. 3. (A) Association of baseline luminal MWS and WSS with ΔWT in plaque free sectors. (B) Association of baseline luminal MWS and WSS with ΔWT in plaque sectors. (C) Association of combinations of baseline luminal MWS and WSS with ΔWT, stratified by LRNC presence, in plaque sectors based on Linear Mixed Model. (Data are presented as mean with 95% CI. MWS: mechanical wall stress; WSS: wall shear stress, and ΔWT: wall thickness change,***: $p < 0.001$, **: $p < 0.01$, *: $p < 0.05$).

Plaque sectors without LRNC had higher WT reduction over time compared to plaque sectors with LRNC. Higher luminal MWS was associated with higher WT reduction over time ($p = 0.02$) (Fig. 3B). A similar trend was also observed between WSS and ΔWT. Sectors exposed to higher WSS demonstrated higher WT reduction ($p < 0.001$) (Fig. 3B).

The interaction term of WSS, luminal MWS, and LRNC presence on ΔWT revealed a significant combined effect ($p = 0.02$). The smallest ΔWT was observed in the plaque sectors that were exposed to low luminal MWS and low WSS (Fig. 3C). The highest WT reduction was observed for the sectors exposed to high luminal MWS and high WSS. For any combination of the luminal MWS and WSS, the plaque sectors with no LRNC demonstrated higher ΔWT than the sectors with LRNC (Fig. 3C).

3.3. Plaque composition change and biomechanics

Plaque sectors showed a mean ΔLRNC of 54% reduction, 95% CI [-64%, −43%]. Eighty-five percent of the sectors showed a decrease in LRNC percentage over time. More detailed LRNC measurements at baseline and follow-up are provided in the Supplementary data.

The linear mix models, while correcting for baseline LRNC percentage, revealed that luminal MWS ($p = 0.022$), WSS ($p = 0.004$), and their interaction ($p = 0.003$) were statistically significantly associated with LRNC percentage change over time (ΔLRNC (%)). Specifically, luminal MWS presented a negative trend while WSS presented a positive trend towards LRNC percentage change within plaque sectors (Fig. 4A). The combination of low baseline luminal MWS and high baseline WSS was associated with % LRNC increase whereas high baseline luminal MWS and low baseline WSS with possible % LRNC reduction (Fig. 4B).

4. Discussion

The current study presents the investigation of the individual and synergistic effect of MWS and WSS on coronary atherosclerosis. The

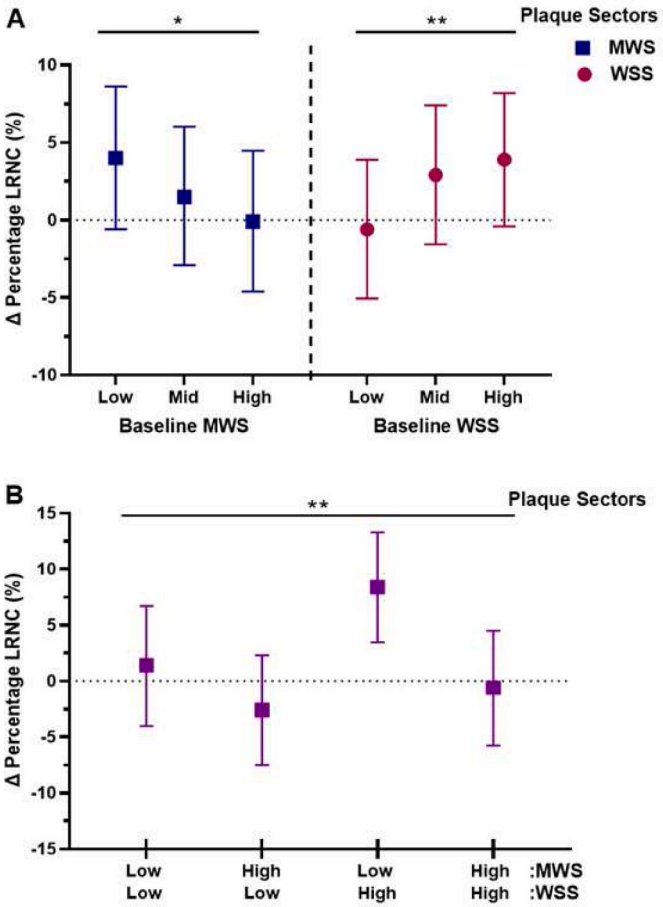

Fig. 4. (A) Association of baseline luminal MWS and WSS levels on Δ LRNC (%) in plaque sectors based on Linear Mixed Model. (B) Association of the interaction effect of baseline luminal MWS and WSS on Δ LRNC (%) based on Linear Mixed Model. (Data are presented as mean with 95% CI. MWS: mechanical wall stress; WSS: wall shear stress, and Δ LRNC: lipid-rich necrotic core change, **: $p < 0.01$, *: $p < 0.05$).

measurements revealed that at the baseline the majority of the arterial sectors were plaque free and the majority of the plaque sectors did not contain LRNC as the selected arteries were non-culprit with moderate lesions. During the one-year follow-up time, many plaque-free sectors thickened whereas many plaque sectors got thinner and reduced their LRNC content. This is likely due to the effect of statin treatment. Statins are known for their lipid-lowering [24] and plaque regression effect even within six months after therapy initiation [25].

Low WSS in human coronary arteries had been shown before to associate greatly with atherosclerotic plaque initiation and progression [26–28]. Our study confirms these findings, as WSS in plaque-free and plaque sectors followed a negative trend with low WSS causing the highest plaque initiation and lowest plaque regression, respectively. According to Conway et al. [5], low WSS triggers athero-inflammatory pathways, such as the downregulation of nitric oxide, through endothelial cell deformation. In addition, our finding on the association of high WSS in plaque sectors with high plaque regression is in line with the finding of the study by Samady et al. [29], where high WSS in human coronary arteries was shown to be associated with fibrous and fibrofatty tissue reduction, suggesting a potential plaque regression mechanism.

Besides WSS, we also looked in our study at the other biomechanical factor in the arterial system, the MWS, which has been mainly overlooked with regard to atherosclerotic disease development. MWS is affected by the blood pressure and the local structural geometry. Our findings show that plaque-free sectors with high MWS present the highest wall thickness increase over time. Previous in-vitro studies have demonstrated various atherosclerosis-related mechanobiological pathways may depend on MWS levels on the lumen surface and/or within the vessel wall [30]. Luminal MWS has a direct biomechanical impact on the endothelial cell stretch state. Hirata et al. demonstrated that uniaxial stretching of human umbilical endothelial cells enhanced the expression of endothelial lipase, a protein with a crucial role in regulating lipid metabolism and promoting atherosclerosis development [31]. Uniaxial [32] and biaxial [33] cyclic stretch of endothelial cells were also shown to promote inflammatory response and thrombogenicity through the NF-κB -COX pathway. Whereas the luminal MWS affects the endothelial cells, the within-vessel wall MWS is likely to impact the deeper arterial wall layers, structures, and cells, such as smooth muscle cells. According to Humphrey et al. [19], high circumferential (intramural) wall stress caused by hypertension in the arterial tissue increases extracellular matrix synthesis by stimulating smooth muscle cells, potentially via the increased local production of angiotensin-II. Smooth muscle cells from mouse aortas were shown to present, when subjected to stretch, a stress-induced inflammatory response through NF-κB signal transduction pathways which may lead to plaque formation [34]. Moreover, rat aortic smooth muscle cells exposed to cyclic stretch or high-pressure condition was shown to demonstrate enhanced cell proliferation [35–37]. It is important to note that in our study the luminal MWS and the within-vessel MWS in plaque free sectors were closely correlated. Hence, the trends between ΔWT and the luminal MWS, and between ΔWT and the within-vessel MWS were very similar for the plaque-free sectors (data not shown). This unfortunately prevents us from hinting towards any biomechanical trigger mechanism in regards to MWS involvement in atherosclerosis initiation and if the mechanism(s) involve endothelial cells or deeper wall structures and cells, or both.

Luminal MWS in plaque sectors followed the opposite trend compared to plaque-free sectors, reflecting the influence of plaque composition and geometry on wall structural stress. In our study, high luminal MWS was associated with the highest plaque thickness reduction. Similarly, Costopoulos et al. [4] showed that high luminal MWS in human coronary arteries was associated with fibrous and fibrofatty tissue reduction. Our study further illustrated the importance of the combined effect of WSS and luminal MWS toward wall thickness change. An interesting finding of our study is that the combination of high WSS and high luminal MWS resulted in the highest wall thickness reduction, reflecting their synergistic effect on plaque regression. It seems that, of these sectors, in the ones with LRNC, the plaque regression was not mainly due to the reduction in LRNC content. Furthermore, our finding that plaque sectors with LRNC exposed to high WSS and low luminal MWS presenting moderate wall thickness reduction but the highest LRNC percentage increase may imply the transformation of these sectors into a higher-risk phenotype [38,39].

In this study, there are a few limitations we need to consider. Firstly, the presence of calcification in cross-sections hindered the visualization of the outer vessel wall layer (external elastic lamina), hence the construction of the cross-section geometry. Therefore, our study was limited to non-calcified cross-sections. In addition, cross-sections exactly at the side branches could not be analyzed since the FE models required complete intactness in the circumference. Secondly, the segmentation of the outer edge of LRNCs was not possible with the combined NIRS-IVUS and OCT imaging approach. Therefore, a previously reported and validated [23] approach was used to reconstruct the LRNC outer edges. Any possible inaccuracy in this reconstruction is expected to have no or minimal effect on the MWS, especially the luminal MWS as the reconstructed edge of the LRNC is far away from the lumen. Thirdly, the patient cohort was under statin treatment. Statins lower the level of low-density lipoprotein cholesterol in the blood and reduce the inflammation within the vessel wall hindering the natural development of atherosclerosis disease. The CFD simulations were performed with rigid wall and no cardiac motion assumptions [21], which were illustrated to have negligible effects on WSS [40].

4.1. Conclusion

In the current study we investigated the association between coronary MWS, individually and combined with WSS, and atherosclerosis development. Our study demonstrated significant associations of both WSS and MWS, the latter having been largely overlooked so far, to plaque formation and development in the non-calcified coronary artery segments (Fig. 5). In plaque-free sectors, MWS was positively and WSS was negatively correlated with vessel wall growth. Overall, plaque sectors demonstrated a reduction in vessel wall thickness over time, likely due to the statin treatment, where the sectors with low MWS and/or low WSS demonstrated the least WT reduction. Moreover, MWS and WSS were also associated with plaque composition change. MWS was negatively and WSS was positively correlated with relative LRNC size increase.

Financial support

This research was supported by the European Research Council, Brussels, Belgium # 310457. Aikaterini Tziotziou was supported by Erasmus MC MRace grant PhD project.

CRediT authorship contribution statement

Aikaterini Tziotziou: Formal analysis, Software, development, Writing – original draft. **Eline Hartman:** data collection, Formal analysis, Writing – review & editing. **Suze-Anne Korteland:** Software, development, Writing – review & editing. **Aad van der Lugt:** Supervision, Writing – review & editing. **Antonius F.W. van der Steen:** Supervision, Writing – review & editing. **Joost Daemen:** data collection, Writing – review & editing. **Daniel Bos:** Supervision, Writing – review & editing. **Jolanda Wentzel:** Conceptualization, Writing – review & editing. **Ali C. Akyildiz:** Supervision, Conceptualization, Writing – review & editing.

Declaration of competing interest

The authors declare the following financial interests/personal relationships which may be considered as potential competing interests: Joost Daemen received institutional grant/research support from Abbott

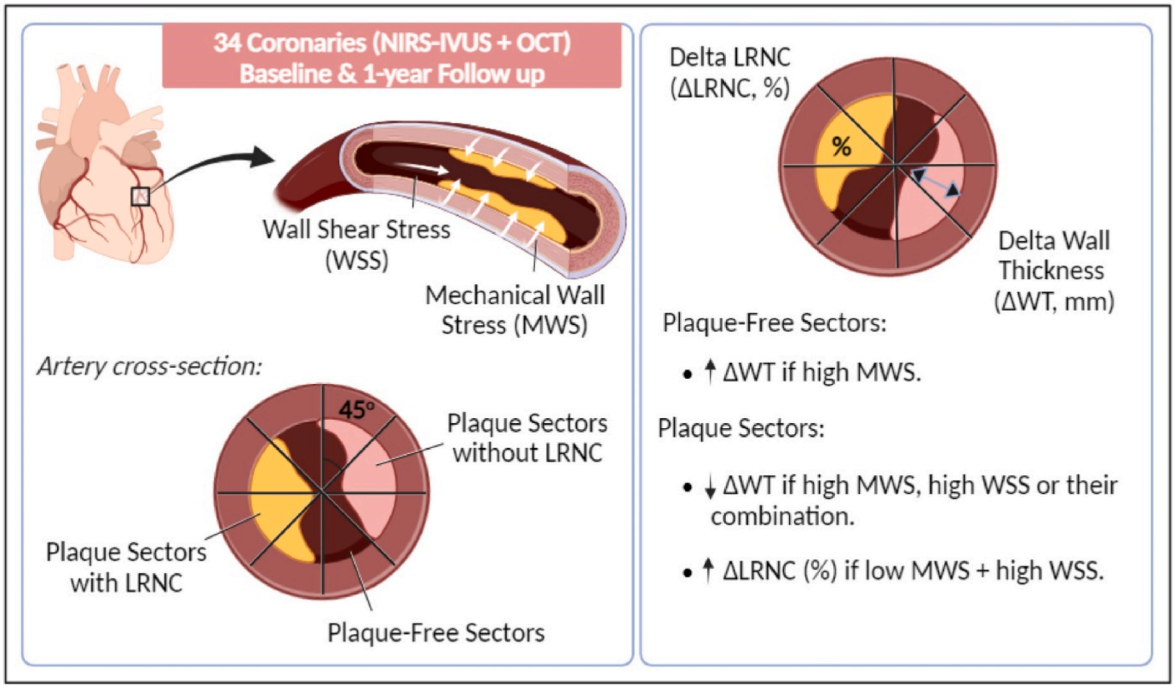

Fig. 5. Graphical abstract.
Both MWS and WSS are significantly associated with plaque formation and development in non-calcified coronary segments.

Vascular, Boston Scientific, ACIST Medical, Medtronic, Microport, Pie Medical, and ReCor medical, and consultancy and speaker fees from Abbott Vascular, Abiomed, ACIST Medical, Boston Scientific, Cardialysis BV, CardiacBooster, Kaminari Medical, ReCor Medical, PulseCath, Pie Medical, Sanofi, Siemens Health Care and Medtronic.

The other authors declare that they have no known competing financial interests or personal relationships that could have appeared to influence the work reported in this paper.

Appendix A. Supplementary data

Supplementary data to this article can be found online at https://doi.org/10.1016/j.atherosclerosis.2023.117387.

References

[1] G.K. Hansson, Inflammation, atherosclerosis, and coronary artery disease, N, Engl. J. Med 352 (2005) 1685–1695, https://doi.org/10.1056/NEJMra043430.
[2] E. Falk, Coronary thrombosis: pathogenesis and clinical manifestations, Am. J. Cardiol. 68 (1991) 28–35, https://doi.org/10.1016/0002-9149(91)90382-U.
[3] R. Diletti, H. Garcia-Garcia, J. Gomez-Lara, et al., Assessment of coronary atherosclerosis progression and regression at bifurcations using combined IVUS and OCT, J. Am. Coll. Cardiol. Img. 7 (2011) 774–780, https://doi.org/10.1016/j.jcmg.2011.04.007.
[4] C. Costopoulos, L.H. Timmins, Y. Huang, et al., Impact of combined plaque structural stress and wall shear stress on coronary plaque progression, regression, and changes in composition, Eur. Heart J. 40 (2019) 1411–1422, https://doi.org/10.1093/eurheartj/ehz132.
[5] D.E. Conway, M.A. Schwartz, Flow-dependent cellular mechanotransduction in atherosclerosis, J. Cell Sci. 126 (2013) 5101–5109, https://doi.org/10.1242/jcs.138313.
[6] Y. Chatzizisis, A. Coskun, M. Jonas, et al., Role of endothelial shear stress in the natural history of coronary atherosclerosis and vascular remodeling, J. Am. Coll. Cardiol. 25 (2007) 2379–2393, https://doi.org/10.1016/j.jacc.2007.02.059.
[7] A. Shaaban, A. Duerinckx, Wall shear stress and early atherosclerosis, AJR (Am. J. Roentgenol.) 174 (2000) 1657–1665, 1657-65.10.2214/ajr.174.6.1741657.
[8] V. Peiffer, S.J. Sherwin, P.D. Weinberg, Does low and oscillatory wall shear stress correlate spatially with early atherosclerosis? A systematic review, Cardiovasc. Res. 99 (2013) 242–250, https://doi.org/10.1093/cvr/cvt044.
[9] J.J. Wentzel, J.C. Schuurbiers, N. Gonzalo Lopez, et al., In vivo assessment of the relationship between shear stress and necrotic core in early and advanced coronary artery disease, EuroIntervention 9 (2013) 989–995, https://doi.org/10.4244/EIJV9I8A165.
[10] P. Eshtehardi, M.C. McDaniel, J. Suo, et al., Association of coronary wall shear stress with atherosclerotic plaque burden, composition, and distribution in patients with coronary artery disease, J. Am. Heart Assoc. 4 (2012), e002543, https://doi.org/10.1161/JAHA.112.002543.
[11] A.C. Akyildiz, L. Speelman, H.A. Nieuwstadt, et al., The effects of plaque morphology and material properties on peak cap stress in human coronary arteries, Comput, Methods Biomech. Biomed. Eng. 19 (2016) 771–779, https://doi.org/10.1080/10255842.2015.1062091.
[12] A.C. Akyildiz, L. Speelman, H. van Brummelen, et al., Effects of intima stiffness and plaque morphology on peak cap stress, Biomed. Eng. Online 10 (2011) 25, https://doi.org/10.1186/1475-925X-10-25.
[13] A.J. Brown, Z. Teng, P.C. Evans, et al., Role of biomechanical forces in the natural history of coronary atherosclerosis, Nat. Rev. Cardiol. 13 (2016) 210–220, https://doi.org/10.1038/nrcardio.2015.203.
[14] G.C. Cheng, H.M. Loree, R.D. Kamm, et al., Distribution of circumferential stress in ruptured and stable atherosclerotic lesions. A structural analysis with histopathological correlation, Circulation 87 (1993) 1179–1187, https://doi.org/10.1161/01.CIR.87.4.1179.
[15] D. Tang, Z. Teng, G. Canton, et al., Sites of rupture in human atherosclerotic carotid plaques are associated with high structural stresses: an in vivo MRI-based 3D fluid-structure interaction study, Stroke 40 (2009) 3258–3263, https://doi.org/10.1161/STROKEAHA.109.558676.
[16] H. Gao, Q. Long, D.S. Kumar, et al., Study of carotid arterial plaque stress for symptomatic and asymptomatic patients, J. Biomech. 44 (2011) 2551–2557, https://doi.org/10.1016/j.jbiomech.2011.07.012.
[17] R. Virmani, A. Burke, A. Farb, et al., Pathology of the vulnerable plaque, J. Am. Coll. Cardiol. 47 (2006) 13–18, https://doi.org/10.1016/j.jacc.2005.10.065.
[18] J. Ohayon, G. Finet, A.M. Gharib, et al., Necrotic core thickness and positive arterial remodeling index: emergent biomechanical factors for evaluating the risk of plaque rupture, Am. J. Physiol. Heart Circ. Physiol. 295 (2008) 717–727, https://doi.org/10.1152/ajpheart.00005.2008.
[19] J.D. Humphrey, D.G. Harrison, C.A. Figueroa, et al., Central artery stiffness in hypertension and aging, Circ. Res. 118 (2016) 379–381, https://doi.org/10.1161/CIRCRESAHA.115.307722.
[20] S. Lee, H. Chang, J. Sung, et al., Effects of statins on coronary atherosclerotic plaques, J. Am. Coll. Cardiol. Img. 11 (2018) 1475–1484, https://doi.org/10.1016/j.jcmg.2018.04.015.
[21] E.M.J. Hartman, G. De Nisco, A.M. Kok, et al., Lipid-rich plaques detected by near-infrared spectroscopy are more frequently exposed to high shear stress, J. Cardiovasc. Trans. Res. 14 (2021) 416–425, https://doi.org/10.1007/s12265-020-10072-x.
[22] E. Conte, S. Mushtaqet, G. Pontone, et al., Plaque quantification by coronary computed tomography angiography using intravascular ultrasound as a reference standard: a comparison between standard and last generation computed tomography scanners, Eur. Heart J – Cardiov. Img. 21 (2020) 191–201, https://doi.org/10.1093/ehjci/jez089.

[23] A.M. Kok, L. Speelman, R. Virmani, et al., Peak cap stress calculations in coronary atherosclerotic plaques with an incomplete necrotic core geometry, Biomed. Eng. Online 15 (2016) 48, https://doi.org/10.1186/s12938-016-0162-5.
[24] M.A. Shuhaili, I.N. Samsudin, J. Stanslas, et al., Effects of different types of statins on lipid profile: a perspective on asians, Int. J. Endocrinol. Metabol. 22 (2017), e43319, https://doi.org/10.5812/ijem.43319.
[25] M.S. Bittencourt, R.J. Cerci, Statin effects on atherosclerotic plaques: regression or healing? BMC Med. 13 (2015) 260, https://doi.org/10.1186/s12916-015-0499-9.
[26] C.V. Bourantas, T. Zanchin, A. Sakellarios, et al., Implications of the local haemodynamic forces on the phenotype of coronary plaques, Heart 105 (2019) 1078–1086, https://doi.org/10.1136/heartjnl-2018-314086.
[27] P.H. Stone, S. Saito, S. Takahashi, et al., Prediction of progression of coronary artery disease and clinical outcomes using vascular profiling of endothelial shear stress and arterial plaque characteristics: the prediction study, Circulation 126 (2012) 172–181, https://doi.org/10.1161/CIRCULATIONAHA.112.096438.
[28] A. Hoogendoorn, A.M. Kok, E.M.J. Hartman, et al., Multidirectional wall shear stress promotes advanced coronary plaque development: comparing five shear stress metrics, Cardiovasc. Res. 116 (2020) 1136–1146, https://doi.org/10.1093/cvr/cvz212.
[29] H. Samady, P. Eshtehardi, M.C. McDaniel, et al., Coronary artery wall shear stress is associated with progression and transformation of atherosclerotic plaque and arterial remodeling in patients with coronary artery disease, Circulation 124 (2011) 779–788, https://doi.org/10.1161/CIRCULATIONAHA.111.021824.
[30] E.C. Viel, C.A. Lemarie, K. Benkirane, et al., Immune regulation and vascular inflammation in genetic hypertension, Am. J. Physiol. Heart Circ. Physiol. 298 (2010) 938–944, https://doi.org/10.1152/ajpheart.00707.2009.
[31] K. Hirata, T. Ishida, H. Matsushita, et al., Regulated expression of endothelial cell-derived lipase, Biochem. Biophys. Res. Commun. 272 (2000) 90–93, https://doi.org/10.1006/bbrc.2000.2747.
[32] T. Korff, K. Aufgebauer, M. Hecker, Cyclic stretch controls the expression of cd40 in endothelial cells by changing their transforming growth factor-beta 1 response, Circulation 116 (2007) 2288–2297, https://doi.org/10.1161/circulationaha.107.730309.
[33] H. Zhao, T. Hiroi, B.S. Hansen, et al., Cyclic stretch induces cyclooxygenase-2 gene expression in vascular endothelial cells via activation of nuclear factor kappa-beta, Biochem. Biophys. Res. Commun. 389 (2009) 599–601, https://doi.org/10.1016/j.bbrc.2009.09.028.
[34] A. Zampetaki, Z. Zhang, Y. Hu, et al., Biomechanical stress induces il-6 expression in smooth muscle cells via ras/rac1-p38 mapk-nf-b signaling pathways, Am. J. Physiol. Heart Circ. Physiol. 288 (2005) 2946–2954, https://doi.org/10.1152/ajpheart.00919.2004.
[35] Z.Y. Zhang, M. Zhang, Y.H. Li, et al., Simvastatin inhibits the additive activation of erk1/2 and proliferation of rat vascular smooth muscle cells induced by combined mechanical stress and oxldl through lox-1 pathway, Cell. Signal. 25 (2013) 332–340, https://doi.org/10.1016/j.cellsig.2012.10.006.
[36] L. Sun, K. Niwa, J.Z. Lin, et al., Cellular growth under hydrostatic pressure using bovine aortic ec-smc co-cultured eptfe vascular graft, J. Zhejiang Univ. - Sci. B. 6 (2005) 79–82, https://doi.org/10.1631/jzus.2005.B0079.
[37] M. Watase, M.A. Awolesi, J. Ricotta, et al., Effect of pressure on cultured smooth muscle cells, Life Sci. 61 (1997) 987–996, https://doi.org/10.1016/s0024-3205(97)00603-6.
[38] M.T. Corban, P. Eshtehardi, J. Suo, et al., Combination of plaque burden, wall shear stress, and plaque phenotype has incremental value for prediction of coronary atherosclerotic plaque progression and vulnerability, Atherosclerosis 232 (2014) 271–276, https://doi.org/10.1016/j.atherosclerosis.2013.11.049.
[39] R. Waksman, C. Di Mario, R. Torguson, et al., Identification of patients and plaques vulnerable to future coronary events with near-infrared spectroscopy intravascular ultrasound imaging: a prospective, cohort study, Lancet 394 (10209) (2019) 1629–1637, https://doi.org/10.1016/S0140-6736(19)31794-5.
[40] R. Torii, J. Keegan, N.B. Wood, et al., MR image-based geometric and hemodynamic investigation of the right coronary artery with dynamic vessel motion, Ann. Biomed. Eng. 38 (2010) 2606–2620, https://doi.org/10.1007/s10439-010-0008-4.